Structural study of magnesioaxinite and its crystal-chemical relations with axinite-group minerals

Article *in* European Journal of Mineralogy · November 2000

CITATIONS
14

READS
79

3 authors, including:

Giovanni B Andreozzi
Sapienza University of Rome
108 PUBLICATIONS **1,621** CITATIONS

SEE PROFILE

Eur. J. Mineral.
2000, **12**, 1185-1194

Structural study of magnesioaxinite and its crystal-chemical relations with axinite-group minerals

GIOVANNI B. ANDREOZZI, SERGIO LUCCHESI* and GIORGIO GRAZIANI

Dipartimento di Scienze della Terra, Università di Roma "La Sapienza", P.le A. Moro 5, I-00185 Roma, Italy

Abstract: The magnesium end-member of the axinite mineral group was studied by single-crystal X-ray diffraction and refined in the $P\bar{1}$ space group (R = 2.2 %). Cell parameters are a = 7.1381(3) Å, b = 9.1626(4) Å, c = 8.9421(4) Å, α = 91.903(4)°, β = 98.105(3)°, γ = 77.468(4)°, V = 565.21(4) Å^3. Magnesioaxinite is isostructural with (Mn,Fe)-axinites, but shows structural features which may account for the compositional gap observed between magnesioaxinite and manganaxinite.

Electron and ion microprobe analyses and refined site occupancies gave the following crystal chemical formula: $^{[6]}[Ca_{2.00}(Ca_{1.95}Mn_{0.03})(Mg_{1.92}Mn_{0.04}V_{0.03}Cr_{0.01})Al_{2.00}Al_{2.00}]^{[4]}[B_{2.01}Si_{8.02}O_{30}](OH_{1.9}O_{0.1})$, very close to the ideal Mg end-member. The octahedron occupied by Mg (<Mg-O> = 2.17 Å) is distorted and closely connected with both tetrahedral and octahedral structure components. Its modification (when Mg substitutes for Fe^{2+} and Mn) causes lattice deformations and also influences T-O-T angles and geometry of octahedral sheets.

Key-words: borosilicates, axinite, magnesioaxinite, crystal structure, crystal chemistry.

Introduction

The axinite-group minerals are borosilicates commonly occurring as accessory phases in skarn and other contact metamorphic rocks (Grew, 1996, and references therein). Moreover, as in some localities they are the only borosilicates in regionally metamorphosed rocks, axinites are believed to be alternative to tourmalines in Al-poor, Ca-rich parageneses at low temperature (Pringle & Kawachi, 1980). Their chemical composition is characterised by variable Mn, Fe, Mg contents, $Fe^{3+}/\Sigma Fe$ ratios and by the presence of B and H as constituent elements. The structural formula $(Ca,Mn)_4(Mn,Fe,Mg)_2Al_4B_2Si_8O_{30}(OH)_2$ was proposed by Sanero & Gottardi (1968), who also defined the nomenclature for the different members of the group. When calcium is close to 4 atoms per formula unit (apfu), the end-members manganaxinite, ferroaxinite and magnesioaxinite depend upon Mn, Fe^{2+} and Mg contents. In the end-member tinzenite ($2 \leq Ca \leq 4$ apfu), Mn excess (> 2 apfu) substitutes for Ca (Milton *et al.*, 1953; Basso *et al.*, 1973; Belokoneva *et al.*, 1997).

The crystal structure of axinite was solved in $P\bar{1}$ by Ito *et al.* (1969) and refined by Takéuchi *et al.* (1974). Axinite structure was described as a sequence of layers, almost parallel to $(\bar{1}21)$, formed by tetrahedrally- and octahedrally-coordi-

* E-mail: SERGIO.LUCCHESI@UNIROMA1.IT

0935-1221/2000/0012-1185 $ 2.50

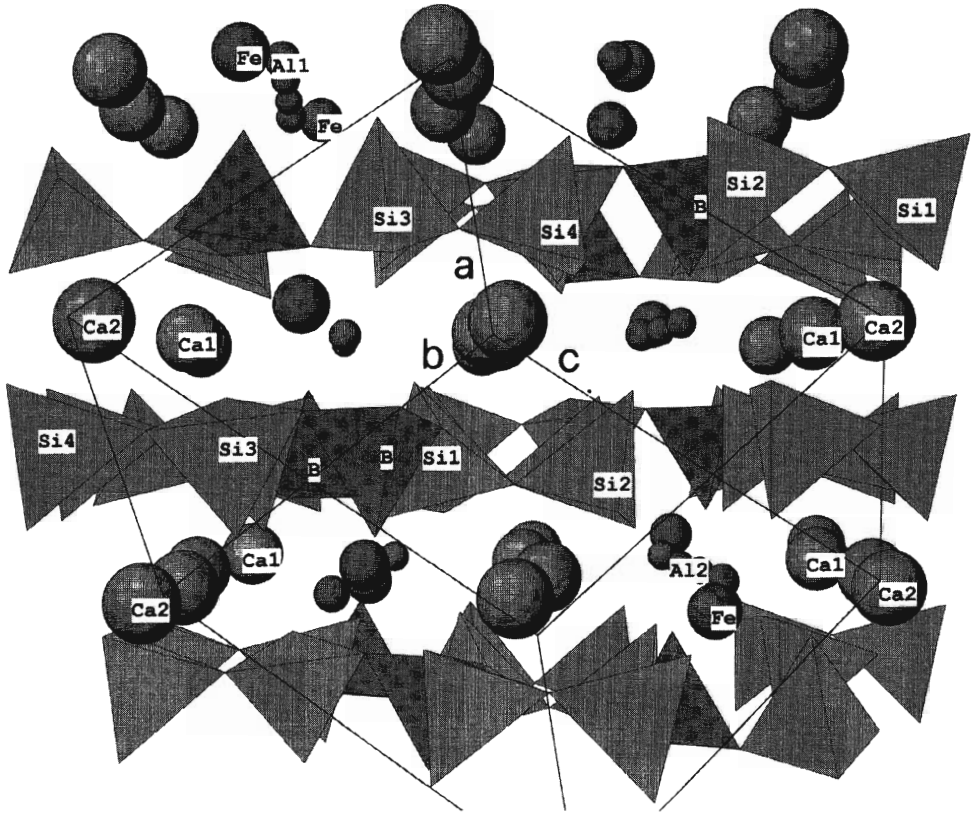

Fig. 1. Crystal structure of axinite as seen approximately along [211]. Note evident tetrahedral and octahedral layers, the former represented by coordination polyhedra, the latter by atoms. Si-centred tetrahedra: light grey; B-centred tetrahedra: medium grey.

nated cations (Fig. 1). Corner-sharing tetrahedra Si(1) and Si(2) form two disilicate groups [Si_2O_7], which are connected by two BO_4 tetrahedra to form a six-membered ring. Two additional disilicate groups, made up of Si(3) and Si(4) tetrahedra, share corners with the BO_4 tetrahedra, forming a [$B_2Si_8O_{30}$] planar cluster (Fig. 2a). The [$B_2Si_8O_{30}$] groups are not linked to each other and constitute the interrupted tetrahedral layer (Fig. 2b). Slightly distorted octahedra (Fig. 3a) share edges to form a six-fold finite chain, (Mn,Fe,Mg)-Al(1)-Al(2)-Al(2)-Al(1)-(Mn,Fe,Mg). These chains are almost parallel to [211], and lateral connection among them is provided by strongly distorted Ca(1) and Ca(2) octahedra (Fig. 3a). As a result, continuous octahedral sheets are formed (Fig. 3b) and tetrahedral layers are sandwiched between them (Fig. 1). The hydrogen atom is bonded to O(16), which is shared by Al(1), Al(2) and Ca(2), and forms a hydrogen bridge with O(13). The structure of tinzenite, the Ca-deficient member of the group, was refined by Basso *et al.* (1973). Results of this

Fig. 2. Tetrahedral sites in axinite structure; projection plane near ($\bar{1}21$). Si-centred tetrahedra: light grey; B-centred tetrahedra: medium grey. a) [$B_2Si_8O_{30}$] cluster; a black circle marks position of inversion centre. b) Interrupted tetrahedral layer.

Fig. 3. Octahedral sites in axinite structure; projection plane near ($\bar{1}21$). Mg-centred octahedra: dark grey; Al-centred octahedra: medium grey; Ca-centred octahedra: light grey. a) Mg...Mg chain with adjoining Ca octahedra; a black circle between the two Al(2) octahedra marks position of inversion centre. b) Octahedral sheet; "A" identifies the lozenge-shaped cavities separating the Mg...Mg chains.

Fig. 2a

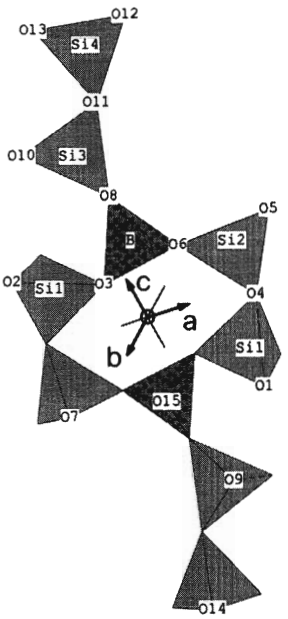

Fig. 2b

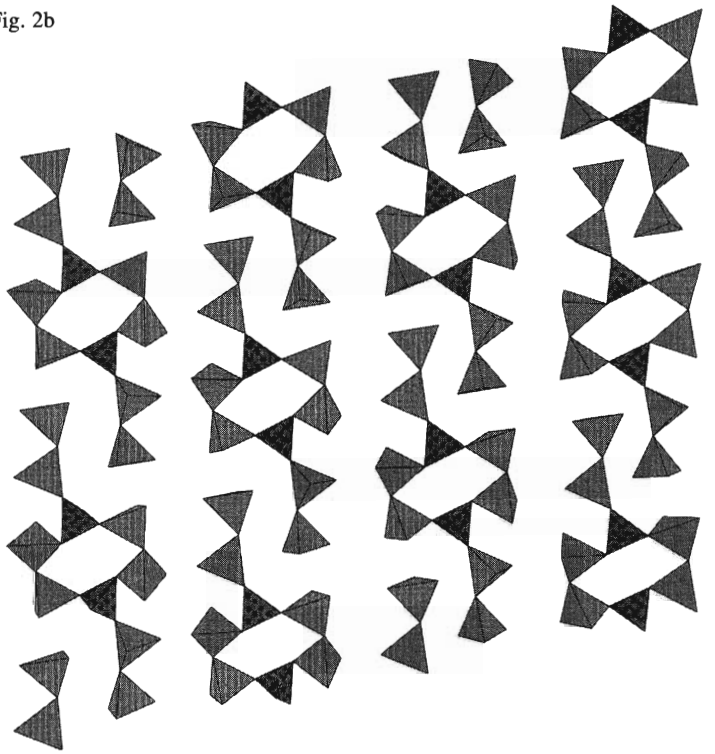

Fig. 3a

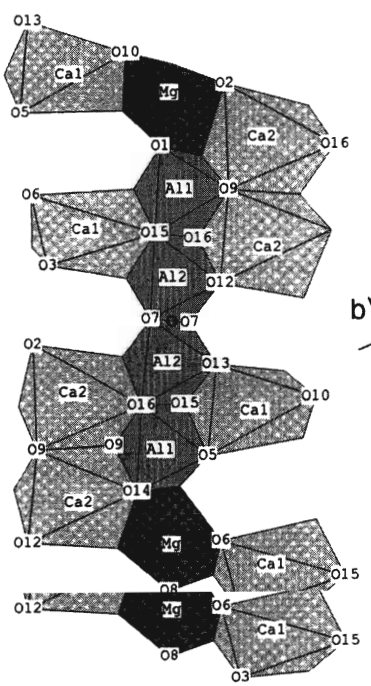

Fig. 3b

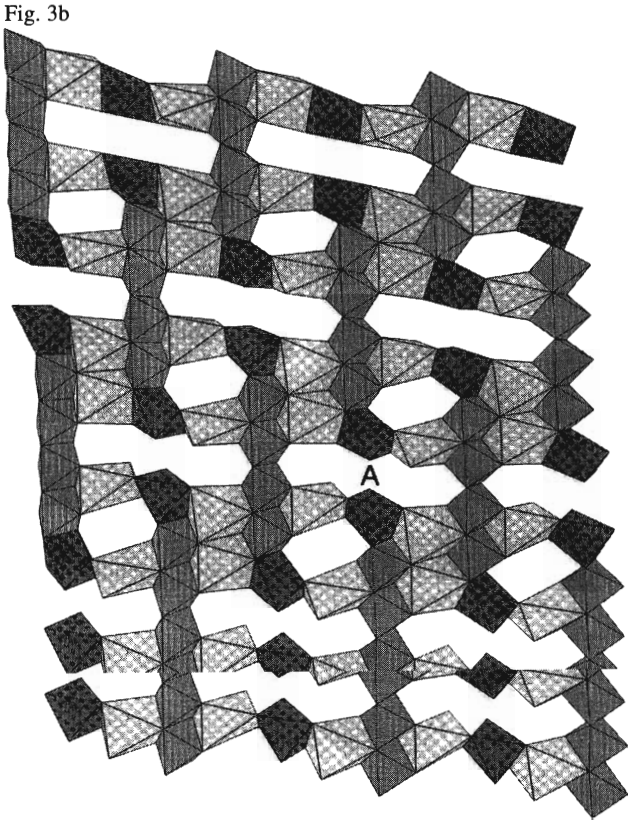

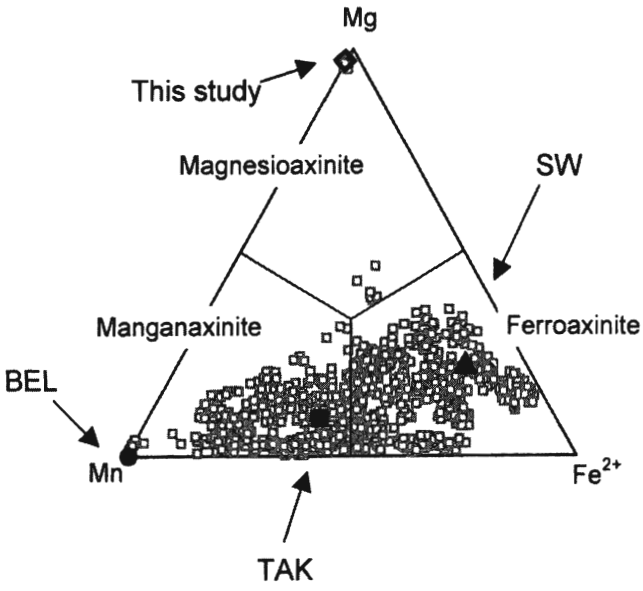

Fig. 4. Mn-Fe^{2+}-Mg contents of axinites [normalised to (Mn + Fe^{2+} + Mg) = 1] and their distribution in subfields of manganaxinite, ferroaxinite and magnesioaxinite (after Andreozzi *et al.*, 2000). Compositional gap between manganaxinite and magnesioaxinite is evident. Open diamond: this study; full circle: sample BEL (Belokoneva *et al.*, 1997); full square: sample TAK (Takéuchi *et al.*, 1974); full triangle: sample SW (Swinnea *et al.*, 1981). Tinzenite BAS (Basso *et al.*, 1973) cannot be properly represented in this diagram, however its position would plot at the Mn corner.

work confirmed the model of Ito *et al.* (1969) and revealed the excess of Mn atoms ordered in Ca(2), the smaller of the two independent Ca-octahedra.

The crystal chemistry of axinites was considered by Lumpkin & Ribbe (1979) and revised in Andreozzi *et al.* (2000), who proposed the general formula for the group:
$^{[6]}[Ca(Ca_{1-x}Mn_x)(Mn,Fe^{2+},Mg,Zn,Al_u,Fe^{3+}_v)_{\Sigma=1}(Al_{2-y}Fe^{3+}_y)]_2{}^{[4]}[(B_{1-z}Si_z)_2Si_8]O_{30}(OH_{1-w}O_w)_2$,
where $x \leq 1$, $u << 1$, $v << 1$, $y < 1$, $z << 1$ and $w = (u + v + z)$.

Ferroaxinites and Mg-poor manganaxinites are the compositions most frequently found, whereas magnesioaxinites are rarer and generally limited to compositions close to the boundary with the ferroaxinite (Fig. 4). The only known specimens close to the magnesioaxinite end-member are gem-quality crystals from Tanzania (Jobbins *et al.*, 1975; Andreozzi *et al.*, 2000).

The large compositional gap existing between the Mg and Mn end-members of axinite group (Fig. 4) was first observed by Chaudhry & Howie (1969) and Pringle & Kawachi (1980), and further emphasised by Andreozzi *et al.* (2000). This gap may be due to the scarcity of rocks simultaneously impoverished in Fe and enriched in Mn, Mg and B or also to the tendency of axinites to fractionate Mn and Fe (Grew, 1996). Whether the absence of solid solution between manganaxinite and magnesioaxinite is also due to structural constraints still remains to be clarified. Since the only two axinites refined so far are intermediate (Mn-Fe) samples, the framework details of the three end-members, particularly Mg, need to be clarified. Consequently, a structural study on the end-member magnesioaxinite is of fundamental importance for the definition of the crystal chemistry of the axinite group minerals.

Materials and methods

The specimen studied consists of a light-blue, gem-quality idiomorphic crystal (approximately 10 x 9 x 6 mm) kindly provided by Dr. J. Saul to one of the authors (G.G.). This magnesioaxinite was found in the Merelani Hills, south of Arusha, Tanzania, with diopside, gem-quality blue zoisite (tanzanite) and green grossular garnet (tsavorite) (J. Saul, personal communication). The embedding rocks consist primarily of graphite-bearing gneisses and marbles. Magnesioaxinite crystals show the typical axe-shaped habit, with a well-developed {010} pinacoid with evident [001] striae. Refractive indexes $\alpha = 1.650(2)$, $\beta = 1.660(2)$ and $\gamma = 1.670(2)$ were measured by the immersion method using a universal stage. Density was measured at 294 K with a Berman balance.

X-ray diffraction data (Table 1) were collected using a Siemens P4 four-circle automated X-ray diffractometer at 298 K. The unit cell parameters were refined by collecting 13 independent reflections (at $\pm 2\theta$) and their Friedel pairs (Mo$K\alpha_1$ radiation, λ = 0.70930 Å) in the range 85-95° 2θ.

Table 1. Magnesioaxinite: crystal data and structure determination summary.

Color	Light blue
Habit	pinacoidal
Crystal size (mm)	0.2×0.3×0.3
Space group	$P\bar{1}$
a (Å)	7.1381(3)
b (Å)	9.1626(4)
c (Å)	8.9421(4)
α (°)	91.903(4)
β (°)	98.105(3)
γ (°)	77.468(4)
Unit cell volume (Å^3)	565.21(4)
Z	2
Density (g/cm^3): obs.	3.16(1)
calc.	3.167
2θ range (°)	3 to 65
Scan type	ω
Scan speed (°/min.)	2.93 to 29.30
Scan range (°)	2.2
Index ranges	$-10 \le h \le 10$
	$-13 \le k \le 13$
	$0 \le l \le 13$
Reflections collected	4320
Observed reflections	4094
Isotropic extinction coeff.	0.0267(7)
N. of parameters refined	244
Final R* index (%)	2.21

* in the form $R = (\Sigma|F_{obs} - F_{calc}|)/(\Sigma F_{obs})$

X-ray diffraction intensities were collected with Mo*K*α radiation (λ = 0.71073 Å). Scan speed was variable and depended on reflection intensity estimated by means of a pre-scan. Background was measured with stationary counter and crystal at the beginning and at the end of each scan, in both cases for half of the scan time. Three standard reflections were monitored every 47 measurements.

Data reduction was performed with the SHELXTL-PC program package. Absorption correction was accomplished with a semi-empirical method, using intensities obtained from the Ψ-scans of 13 non-equivalent reflections in the range 10° - 65° 2θ. Reflections with $I > 2\sigma(I)$ were considered as observed, and the original set of 4320 was reduced to 4094 reflections. Initial fractional coordinates were taken from Takéuchi *et al.* was reduced to 4094 reflections. Initial fractional coordinates were taken from Takéuchi *et al.* (1974). Fully ionised curves were used for all elements. Isotropic secondary extinction was corrected according to Larson's algorithm (Larson, 1970). Three cycles of isotropic full matrix refinements were followed by anisotropic cycles until convergence, with a satisfactory final disagreement factor ($R = 2.2$ %). Final atomic coordinates, refined site scatterings (reported as site mean atomic number) and equivalent-isotropic displacement-parameters (U_{eq}) are listed in Table 2. Position of H atom was localised from inspection of a difference Fourier map; successive isotropic refinement confirmed these coordinates (Table 2), while occupancy was constrained to the value obtained from chemical analysis. The program ATOMS (copyright 1995 by Eric Dowty) was used for drawing structural details. The anisotropic displacement parameters and observed and calculated structure factors may be obtained from authors (or through the E.J.M. Editorial Office - Paris).

The chemical composition of the refined crystal fragment (Table 3) was determined by a multi-analytical approach. Elements with $Z \ge 9$ were analysed by a Cameca SX-50 electron microprobe operated with five wavelength-dispersion (WDS) spectrometers and a Link eXL energy-dispersion system (EDS), both controlled by Specta software, at the "Centro di Studio per il Quaternario e l'Evoluzione Ambientale" C.N.R., Rome. Data were reduced with ZAF-4/FLS software. The natural and synthetic standards used were: wollastonite (Si, Ca), corundum (Al), jadeite (Na), periclase (Mg), fluorphlogopite (F), magnetite (Fe), orthoclase (K), rutile (Ti), and metallic Mn, Cr, V and Zn. Among the examined elements, Fe, Zn, Ti, Na, K and F were not observed since their concentration was below their σ. Analyses for H and B were carried out on the same crystal fragment by means of a Cameca IMS 4f ion microprobe, at the C.N.R.-CSCC, Pavia, with a $^{16}O^-$ primary ion beam. Matrix effects were reduced and reproducibility was improved using the energy-filtering technique (~ 75-125 eV) and measuring the variation of ion yield (IY) for B and H with respect to ^{30}Si, with Si selected as the matrix-reference element (Ottolini *et al.*, 1993). Accuracy for B ≤ 3 % rel. and H ~ 5 % rel. were obtained by calibrating both IY(B/Si) and IY(H/Si) *versus* the (Fe + Mn) contents of each sample included in the experimental calibration curves (more details may be found in Andreozzi *et al.*, 2000).

Results

Results

Chemistry and cell parameters

The chemical composition of the sample

Table 2. Fractional atomic coordinates, mean atomic numbers (m.a.n.) and equivalent displacement parameters (Å²) of magnesioaxinite.

Atom	x	y	z	m.a.n.	U_{eq}
Si(1)	0.21090(5)	0.44980(4)	0.23102(4)	14	0.0040(1)
Si(2)	0.21846(5)	0.27405(4)	0.52188(4)	14	0.0033(1)
Si(3)	0.69967(5)	0.25808(4)	0.01122(4)	14	0.0041(1)
Si(4)	0.64224(5)	0.01769(4)	0.23078(4)	14	0.0037(1)
B	0.4627(2)	0.6347(2)	0.2859(2)	5	0.0049(4)
Al(1)	0.05319(6)	0.79946(5)	0.25516(5)	13.01(3)	0.0037(1)
Al(2)	0.35128(6)	0.93645(5)	0.42062(5)	13.02(3)	0.0040(1)
Mg	0.76596(7)	0.59547(6)	0.11837(5)	12.58(4)	0.0071(2)
Ca(1)	0.74552(4)	0.34737(3)	0.39304(3)	20.05(4)	0.0074(1)
Ca(2)	0.18237(4)	0.10280(3)	0.08373(3)	20.05(4)	0.0082(1)
O(1)	0.0508(1)	0.6024(1)	0.1924(1)	8	0.0052(3)
O(2)	0.2342(2)	0.3428(1)	0.0893(1)	8	0.0069(3)
O(3)	0.4190(1)	0.4867(1)	0.3115(1)	8	0.0053(3)
O(4)	0.1387(2)	0.3674(1)	0.3655(1)	8	0.0091(3)
O(5)	0.0207(1)	0.2418(1)	0.5618(1)	8	0.0051(3)
O(6)	0.3229(1)	0.3802(1)	0.6462(1)	8	0.0050(3)
O(7)	0.3817(1)	0.1268(1)	0.4968(1)	8	0.0047(3)
O(8)	0.5333(1)	0.3422(1)	0.8767(1)	8	0.0050(3)
O(9)	0.8773(1)	0.1563(1)	0.9328(1)	8	0.0050(3)
O(10)	0.7686(2)	0.3727(1)	0.1355(1)	8	0.0071(3)
O(11)	0.6091(2)	0.1340(1)	0.0888(1)	8	0.0085(3)
O(12)	0.4347(1)	0.9825(1)	0.2430(1)	8	0.0049(3)
O(13)	0.7220(1)	0.0986(1)	0.3847(1)	8	0.0048(3)
O(14)	0.7929(2)	0.8695(1)	0.1787(1)	8	0.0061(3)
O(15)	0.3255(1)	0.7458(1)	0.3550(1)	8	0.0041(3)
O(16)	0.0958(1)	0.9955(1)	0.3217(1)	8	0.0047(3)
H	0.989(3)	0.961(2)	0.619(2)	0.95	0.007

closely matches (up to 96 %) ideal magnesioaxinite $Ca_4Mg_2Al_4B_2Si_8O_{30}(OH)_2$ and is very close to that of the sample described by Jobbins *et al.* (1975). In particular, Si, B and Al contents are stoichiometric within the limits of experimental uncertainty (Table 3). The minor content of Mn^{2+} - 0.07(2) apfu - may be added to Mg and Ca to fill their sites. Small contents of V^{3+} and Cr^{3+} were observed over the detection limit and are probably a distinctive feature of Tanzanian axinite, already reported by Jobbins *et al.* (1975).

Unit cell parameters of our magnesioaxinite (Table 1) are not immediately comparable with respect to those of Jobbins *et al.* (1975) since the latter authors used a different cell orientation, which may be transformed into that adopted in the present paper according to the transformation matrix 001/010/100. Our orientation follows that which may be transformed into that adopted in the present paper according to the transformation matrix 001/010/100. Our orientation follows that recommended by Peacock (1937), which is the nearest to the unique set defined by the Eisenstein-reduced lattice and which was adopted in preceding structural studies. A full discussion on the correct choice of axinite unit cell is considered by Salviulo *et al.* (2000).

Structure

The atomic coordinates of magnesioaxinite (Table 2) are close to those of tinzenite (Basso *et al.*, 1973), low-Mn tinzenite (Belokoneva *et al.*, 1997) and two intermediate (Mn,Fe) axinites (Takéuchi *et al.*, 1974; Swinnea *et al.*, 1981). These samples are hereafter identified as BAS, BEL, TAK and SW, respectively.

The four independent tetrahedral sites occupied by Si (Fig. 2a) are characterised by different mean bond distances and site volumes (Table 4). Mean Si-O distances of the inner Si(1) and Si(2) are equal and are significantly smaller than those of the outer Si(3) and Si(4). In particular, Si(2) Mean Si-O distances of the inner Si(1) and Si(2) are equal and are significantly smaller than those of the outer Si(3) and Si(4). In particular, Si(2) shows the smallest site volume. In all four tetrahedra, the Si-O_{br} are longer than Si-$O_{n\,br}$. This is

Table 3. Chemical composition of magnesioaxinite. Average oxide weight percentages and estimated standard deviations (± 1σ).

SiO_2	44.8(2)
B_2O_3*	6.5(2)
Al_2O_3	18.9(3)
V_2O_3	0.23(5)
Cr_2O_3	0.08(2)
MgO	7.18(1)
MnO	0.5(1)
CaO	20.6(1)
H_2O*	1.6(1)
Total	100.4
Ions on the basis of 32 (O,OH)	
Si	8.02(4)
B	2.01(5)
Al	3.99(3)
V^{3+}	0.033(6)
Cr^{3+}	0.011(2)
Mg	1.92(1)
Mn	0.07(2)
Ca	3.95(3)
OH	1.9(1)
Total**	20.00

*from ion microprobe
**excluding OH

also reflected by bond valence calculations (parameters by Brown & Altermatt, 1985) which gave mean values ≤ 1 valence unit (v.u.) for Si-O bridging bonds and ≥ 1 v.u. for non-bridging ones.

In order to analyse the deformation of the coordination polyhedra with respect to their ideal geometry, mean quadratic elongation (λ) and angular variance (σ^2) were calculated as defined by Robinson *et al.* (1971). λ values are low and comparable (1.003-1.004) for all tetrahedra except Si(2), which is more distorted (λ = 1.008). In the same way, σ^2 values range between 13.6 and 14.9 for all tetrahedra except Si(2), which shows σ^2 = 32.0. As the mean Si(1) and Si(2) bond distances are identical, the relatively large distortion of the Si(2) tetrahedron provides an explanation for its smaller volume.

Site occupancies were kept fixed during refinement since microanalyses indicated complete occupancy by Si cations (Table 3). Moreover, Al → Si or B → Si substitutions were already excluded for Tanzanian axinite by Andreozzi *et al.* (2000) in their general crystal-chemical study of axinites.

The B tetrahedron is smaller than the Si ones (Table 4) but shows comparable distortion (λ = 1.007, σ^2 = 29.3). Similarly, the three bridging B-O distances are longer than B-O(15), the non-bridging one. Its volume (1.675 Å^3) is characteristic of a site fully occupied by boron (Andreozzi *et al.*, 2000). This is in complete agreement with ion microprobe analysis, which showed boron to be stoichiometric (Table 3). As a consequence, site occupancy was constrained during refinement to full boron content. This assumption is appropriate due to the weak scattering factor of boron and consequently due to the large errors that would have been expected from the analysis of electron density of its site (Hawthorne, 1996).

The two small Al(1) and Al(2) octahedra (Table 5) are almost regular (λ = 1.006 for both; σ^2 = 18.5 and 19.7, respectively) and completely filled by Al, according to site occupancies (Table 2) and microprobe analysis (Table 3). However, both mean bond length and site volume of Al(1) are slightly higher than those of Al(2).

The octahedron surrounding Mg is definitely irregular (λ = 1.067; σ^2 = 177.7) because, similarly to previously refined axinites, two of the six Mg-O bond distances – Mg-O(6) and Mg-O(14) – are longer than the other four (Table 5). Consequently, the Mg-O bond strengths are lower for the former two bonds (0.21 v.u. and 0.09 v.u., respectively) and higher for the latter four (from 0.34 to 0.49 v.u.). The mean atomic number of this site (Table 2) is greater than that expected for full occupancy of Mg, suggesting the presence of heavier cations. In agreement with this observation, Cr^{3+}, V^{3+} and 0.04 apfu Mn^{2+} may be assigned to the Mg site to achieve full occupancy. In this case, charge balance is provided by the sub-stoichiometric OH content (Table 3) according to the coupled substitution $R^{3+}O(MgOH)_{-1}$ (Andreozzi *et al.*, 2000).

The Ca(1) and Ca(2) polyhedra show very high distortion when referred to as octahedra (λ = 1.138 and 1.126; σ^2 = 478.6 and 397.8, respectively), as they should more correctly be described as trigonal antiprisms (Takéuchi *et al.*, 1974). Ca(1) is larger and more distorted than Ca(2) which, according to Basso *et al.* (1973), may contain the remaining minor manganese (0.03 apfu).

Table 4. Interatomic distances (Å) and site volumes (Å^3) of tetrahedra (T) in magnesioaxinite.

	Si(1)	Si(2)	Si(3)	Si(4)	B
O(1)	1.615(1)				
O(2)	1.582(1)				
O(3)	1.655(1)				1.487(2)
O(4)	1.639(1)	1.630(1)			
O(5)		1.593(1)			
O(6)		1.657(1)			1.544(2)
O(7)		1.613(1)			
O(8)			1.647(1)		1.482(2)
O(9)			1.632(1)		
O(10)			1.604(1)		
O(11)			1.640(1)	1.643(1)	
O(12)				1.602(1)	
O(13)				1.632(1)	
O(14)				1.638(1)	
O(15)					1.440(2)
O(16)					
Mean T-O	1.623	1.623	1.631	1.629	1.488
T volume	2.183(2)	2.167(2)	2.214(2)	2.204(2)	1.675(1)

Table 5. Interatomic distances (Å) and site volumes (Å^3) of octahedra (M) in magnesioaxinite.

	Al(1)	Al(2)	Mg	Ca(1)	Ca(2)
O(1)	1.876(1)		2.061(1)		
O(2)			1.959(1)		2.305(1)
O(3)				2.426(1)	
O(4)					
O(5)	1.863(1)			2.347(1)	
O(6)			2.273(1)	2.465(1)	
O(7)		1.897(1)			
		1.915(1)			
O(8)			2.094(1)		
O(9)	1.899(1)				2.357(1)
					2.498(1)
O(10)			2.048(1)	2.355(1)	
O(11)					
O(12)		1.864(1)			2.238(1)
O(13)		1.943(1)		2.319(1)	
O(14)	1.867(1)		2.593(1)		2.404(1)
O(15)	1.986(1)	1.863(1)		2.588(1)	
O(16)	1.946(1)	1.884(1)			2.579(1)
Mean M-O	1.906	1.894	2.171	2.417	2.397
O(16)	1.946(1)	1.884(1)			2.579(1)
Mean M-O	1.906	1.894	2.171	2.417	2.397
M volume	9.155(3)	8.987(3)	12.556(4)	15.532(5)	15.410(5)

The hydrogen atom is bonded to O(16) at 0.88(2) Å and establishes a hydrogen bridge with O(13) at about 2.02 Å, in good agreement with the distances observed by Takéuchi *et al.* (1974) and Swinnea *et al.* (1981).

Discussion

Octahedral sites and role of substitution involving Mg, Fe and Mn

The MgO_6 octahedron has the smallest mean bond length (2.17 Å) compared with the analogous site occupied mainly by Fe or Mn (2.22 Å in SW and BEL, 2.24 Å in BAS and TAK), indicating that the substitution of Mg for (Fe,Mn) causes its contraction. Moreover, with increasing of Mg contents the two longer bonds – Mg-O(6) and Mg-O(14) – decrease more markedly than the other four. As an example, average shortening of Mg-O(6) and Mg-O(14) from TAK to magnesioaxinite is 0.09 Å, compared with 0.05 for the other distances. Consequently, the Mg-centred octahedron is less distorted than its homologues centred by Fe and Mn ($\lambda = 1.067$ and $\sigma^2 = 178$ for magnesioaxinite; $\lambda > 1.080$ and $\sigma^2 > 215$ for the other compositions).

Due to the crucial role played by the $(Mn,Fe,Mg)O_6$ octahedron, its modifications along the manganaxinite-ferroaxinite-magnesioaxinite series cause transformation of the whole structure. In particular, it shares the O(1)-O(14) edge with Al(1) octahedron (Fig. 3a), so that a systematic size decrease of Al(1) may be observed from manganaxinite and ferroaxinite to magnesioaxinite. The Al(1) contraction also determines a size decrease of Al(2), although to a very minor extent. All these transformations produce shortening of the chain of octahedra, which shrinks around the inversion centre located midway along the Al(2)-Al(2) common edge, *i.e.*, O(7)-O(7). Consequently, the length of the chain (measured from Mg to Mg) is 15.02 Å in TAK and 14.88 Å in magnesioaxinite. Moreover, chain contraction causes an enlargement of the lozenge-shaped cavities ("A" in Fig. 3b) in the same direction as the chains and this is reflected by the distance between two consecutive Mg atoms across the cavity which is 4.69 Å in TAK and 4.73 Å in magnesioaxinite.

Lateral distances between rows of chains, governed by Ca polyhedra, are substantially not affected, increasing by about 0.01 Å from TAK to magnesioaxinite. In fact, mean bond distances remain constant in Ca(1) and slightly increase in Ca(2), whereas both octahedra are progressively more deformed.

Tetrahedral sites

The mean bond distances of the tetrahedra remain constant when axinite composition changes in terms of Mn, Fe and Mg, whereas interatomic angles O-T-O and T-O-T reveal that structural changes occur. For example, mean angle Si-O-Si decreases from magnesioaxinite to TAK ranging from 143.4(1)° to 141.3(5)°, respectively. A general trend may be observed in which, the more the T-O-T angle decreases, the more the Si-O bridging distance increases. This confirms the observations of Brown & Gibbs (1970) and Takéuchi *et al.* (1974) who, following Cruickshank (1961), attributed this bond-length variation to the influence of *3d* orbitals on the π-bond between silicon and oxygen atoms.

The mean B-O bond length (1.488 Å) has almost the same value of that of TAK and BEL, and is close to those shown by SW (1.485 Å) and BAS (1.48 Å). This value was found to be characteristic of samples with stoichiometric boron content in the whole axinite compositional field (Andreozzi *et al.*, 2000) so that it does not depend on deformations induced by (Mg,Fe,Mn)-substitutions. Therefore, the value of 1.488 Å may be considered as representing the mean B-O bond length in tetrahedral coordination, at least for axinite.

The strain induced on octahedral sheet by Mg $\rightarrow$ (Fe,Mn) substitution also reflects on the geometry of the $[B_2Si_8O_{30}]$ cluster. In magnesioaxinite, the «ring» defined by B, Si(1) and Si(2) tetrahedra (Fig. 2a) is larger than in the other end-members. This is due to a sharp increase in the O(6)-O(4) edge of the Si(2) tetrahedron (from 2.640 Å in TAK to 2.676 Å in our sample), while the two B and Si(1) tetrahedra behave almost as a rigid body: the result is a more «open» topology in the tetrahedral cluster. Similarly, in the outer portion of the cluster, an increase in the O(10)-O(11)-O(13) angle of about 2° produces an outward rotation of Si(4) with respect to Si(3). Notably, of these three oxygen atoms O(11) is the only one not bonded to the octahedral sheet, whereas O(10) and O(13) are drawn by the deformations of the octahedra.

Conclusions

Conclusions

On the basis of chemical analyses and structural refinement, the crystal chemical formula of Tanzanian magnesioaxinite is:

$^{[6]}[Ca_{2.00}(Ca_{1.95}Mn_{0.03})(Mg_{1.92}Mn_{0.04}V_{0.03}Cr_{0.01})Al_{2.00}Al_{2.00}]^{[4]}[B_{2.01}Si_{8.02}O_{30}](OH_{1.9}O_{0.1})$. Small deviations from full site occupancy are within estimated experimental errors (Table 3).

The presence of Mg in axinite produces a general contraction of the structure due to the role played by the MgO_6 octahedron. Consequently, in the range manganaxinite - ferroaxinite - magnesioaxinite, the lattice parameters show a reduction of up to 0.04 Å in cell edges leading to the maximum difference in cell volume between magnesioaxinite and manganaxinite. A binary solid solution is therefore favoured between magnesioaxinite and ferroaxinite while is expected to be more difficult between magnesioaxinite and manganaxinite. This furthermore suggests that the compositional gap observed in Fig. 4 between manganaxinite and magnesioaxinite is controlled by both geologic and structural constraints.

Acknowledgements: The authors wish to express their gratitude to Dr. J. Saul (Société Oryx, Paris, France) for kindly providing the magnesioaxinite crystal, Dr. M. Martini for refractive indexes and density measurements, Dr. L. Ottolini for ion microprobe analysis, Mr. M. Serracino for assistance during electron microprobe analysis, and Ms. G.Walton for revising the English text. This research was supported by a MURST grant.

References

Andreozzi, G.B., Ottolini, L., Lucchesi, S., Graziani, G., Russo, U. (2000): Crystal chemistry of the axinite-group minerals: A multi-analytical approach. *Am. Mineral.*, **85**, 698-706.

Basso, R., Della Giusta, A., Vlaic, G. (1973): The crystal structure of tinzenite. *Per. Mineral.*, **42**, 369-379 (in Italian).

Belokoneva, E.L., Pletnev, P.A., Spiridonov, E.M. (1997): Crystal structure of low-manganese tinzenite (Severginite). *Crystall. Reports*, **42**, 1010-1013.

Brown, I.D. & Altermatt, D. (1985): Bond-valence parameters obtained from a systematic analysis of the inorganic crystal structure database. *Acta Cryst.*, **B41**, 244-247.

Brown, G.E. & Gibbs, G.V. (1970): Stereochemistry and ordering in the tetrahedral portion of silicates. *Am. Mineral.*, **55**, 1587-1607.

Chaudhry, M.N. & Howie, R.A. (1969): Axinites from the contact skarns of the Meldon aplite, Devonshire, England. *Mineral. Mag.*, **37**, 45-48.

Cruickshank, D.W.J. (1961): The rôle of *3d*-orbitals in the contact skarns of the Meldon aplite, Devonshire, England. *Mineral. Mag.*, **37**, 45-48.

Cruickshank, D.W.J. (1961): The rôle of *3d*-orbitals in π-bonds between (a) silicon, phosphorus, sulphur, or chlorine and (b) oxygen or nitrogen. *J. Chem. Soc.*, 5486-5504.

Grew, E.S. (1996): Borosilicates (exclusive of tourmaline) and boron in rock-forming minerals in metamorphic environments. *in* Mineralogical Society of America *Reviews in Mineralogy*, **33**, 387-502.

Hawthorne, F.C. (1996): Structural mechanisms for light-element variations in tourmaline. *Can. Mineral.*, **34**, 123-132.

Ito, T., Takéuchi, Y., Ozawa, T., Araki, T., Zoltai, T., Finney, S.S. (1969): The crystal structure of axinite revised. *Proc. Japan Academy*, **45**, 490-494.

Jobbins, E.A., Tresham, A., Young, B.R. (1975): Pale blue axinite from East Africa. *J. Gemm.*, **14**, 368-375.

Larson, F.K. (1970): *in* "Crystallographic computing", Ahmed F.R. ed., Munksgaard, Copenhagen.

Lumpkin, G.R. & Ribbe, P.H. (1979): Chemistry and physical properties of axinites. *Am. Mineral.*, **64**, 635-645.

Milton, C., Hildebrand, F.A., Sherwood, A.M. (1953): The identity of tinzenite with manganoan axinite. *Am. Mineral.*, **38**, 1148-1158.

Ottolini, L., Bottazzi, P., Vannucci, R. (1993): Quantification of lithium, beryllium, and boron in silicates by secondary ion mass spectrometry using conventional energy filtering. *Anal. Chem.*, **65**(15), 1960-1968.

Peacock, M.A. (1937): On the crystallography of axinite and the normal setting of triclinic crystals. *Am. Mineral.*, **22**, 588-620.

Pringle, I.J. & Kawachi, Y. (1980): Axinite mineral group in low-grade regionally metamorphosed rocks in southern New Zealand. *Am. Mineral.*, **65**, 1119-1129.

Robinson, K., Gibbs, G.V., Ribbe, P.H. (1971): Quadratic elongation: A quantitative measure of distorsion in coordination polyhedra. *Science*, **172**, 567-570.

Salviulo, G., Andreozzi, G.B., Graziani, G. (2000): X-ray characterization of Mg, Fe and Mn natural end-members of the axinite group. *Powder Diffr.* (in press).

Sanero, E. & Gottardi, G. (1968): Nomenclature and crystal chemistry of axinites. *Am. Mineral.*, **53**, 1407-1411.

Swinnea, J.S., Steinfink, H., Rendon-Diaz Miron, L.E., Enciso de la Vega, S. (1981): The crystal structure of a Mexican axinite. *Am. Mineral.*, **66**, 428-431.

Takéuchi, Y., Ozawa, Y., Ito, T., Araki, T., Zoltai, T., Finney, J.J. (1974): The $B_2Si_8O_{30}$ groups of tetrahedra in axinite and comments on deformation of Si tetrahedra in silicates. *Z. Krist.*, **140**, 289-312.

Received 14 January 2000
Modified version received 12 May 2000
Accepted 16 June 2000